Technology Integration Box Beam Failure Study

M. J. Shuart, D. R. Ambur, D. D. Davis, Jr.,
R. C. Davis, G. L. Farley, C. G. Lotts, and J. T. Wang

NASA Langley Research Center
Hampton, Virginia 23665

Introduction

Composite structures have the potential to be cost-effective, structurally efficient primary aircraft structures. The Advanced Composites Technology (ACT) Program has the goal to develop the technology to exploit this potential for heavily loaded aircraft structures. As part of the ACT Program, Lockheed Aeronautical Systems Company completed the design and fabrication of the Technology Integration Box Beam (TIBB). The TIBB is an advanced composite prototype structure for the center wing section of the C-130 aircraft and is illustrated in figure 1. Lockheed subjected the TIBB to downbending, upbending, torsion and combined upbending and torsion load conditions to verify the design. The TIBB failed at 83 percent of design ultimate load for the combined upbending and torsion load condition.

The objective of this paper is to describe the mechanisms that led to the failure of the TIBB. The results of a comprehensive analytical and experimental study are presented. Analytical results include strain and deflection results from both a global analysis of the TIBB and a local analysis of the failure region. These analytical results are validated by experimental results from the TIBB tests. The analytical and experimental results from the TIBB tests are used to determine a sequence of events that resulted in failure of the TIBB. A potential cause of failure is high stresses in a stiffener runout region. Analytical and experimental results are also presented for a stiffener runout specimen that was used to simulate the TIBB failure mechanisms.

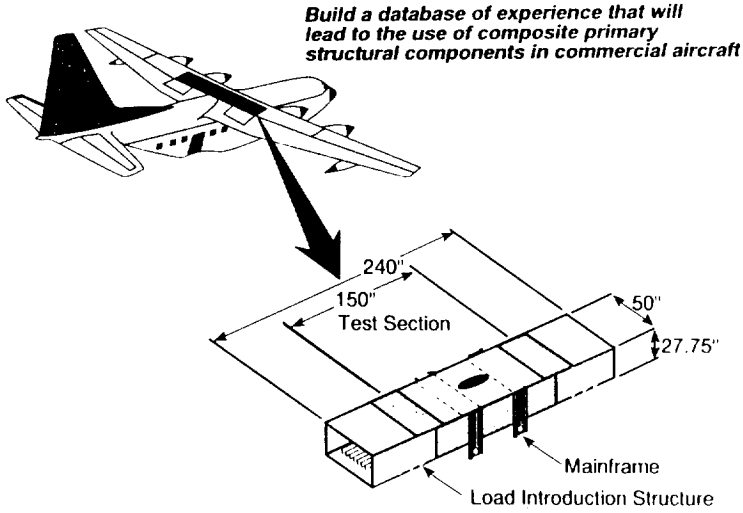

Figure 1

Geometrical Features Contributing to TIBB Failure

Key details of the TIBB geometry are shown in figure 2 to assist in understanding the TIBB response. Discontinuous (or runout) hat stiffeners extend spanwise along the TIBB upper cover panel and are located near the mid-chord of the panel. These stiffeners were included in the design to prevent local buckling and are mechanically fastened and bonded to the upper cover panel skin. The ends of the runout hat stiffeners do not abut against the rib shear ties. Small unstiffened regions of the upper cover panel, or gaps, exist between the flanges of the runout hat stiffeners and the flanges of the rib shear ties. The gap at the end of the hat stiffener closest to the access hole is referred to as Gap 1 and is shown on the figure. The gap at the other end of this hat stiffener is referred to as Gap 2. Gap 2 and Gap 3 are separated by a rib shear tie as shown on the figure. Reinforcing and doubler plates were used in selected regions to add stiffness to the upper cover panel and are also shown on the figure.

The details of the TIBB geometry described above significantly affected the TIBB response. Since the hat stiffener is discontinuous, the location of the neutral axis for the upper cover panel cross-section changes was a function of the spanwise coordinate. The compressive load in the upper cover panel and changing location of the neutral axis cause local bending moments at the ends of the runout hat stiffeners and in the gaps. The gaps do not have reinforcing or doubler plates, and the relatively thin skin in the gaps is subjected to severe bending and compressive strains. The magnitude of the strains in the gaps appears to be a function of both the size of the gap as well as the gap location. The gap strains will be described subsequently in this paper.

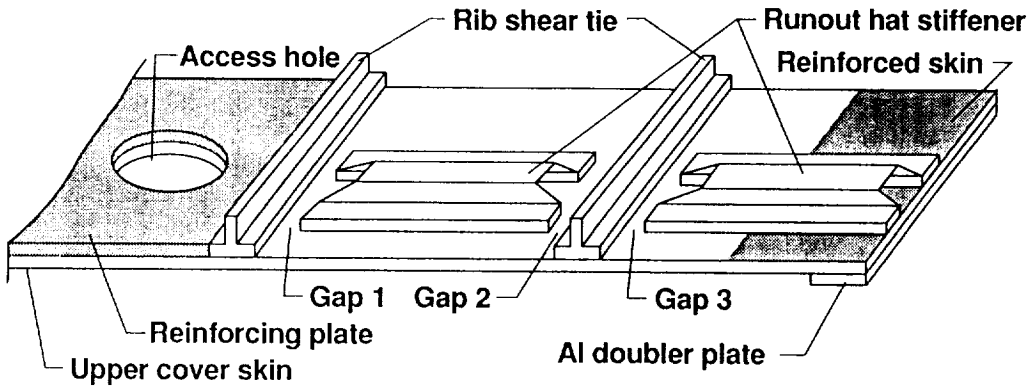

- Load path eccentricities are present at hat stiffener discontinuities
- Stiffened regions adjacent to the gaps channel load into the gaps
- Strain magnitude in a gap is a function of gap size and the proximity of the gap to the stiffened region

Figure 2

Understanding the Response of TIBB

An outline of details needed to understand the TIBB response is given in figure 3. The TIBB was tested in a self-equilibrating test fixture. The ends of the TIBB were loaded by hydraulic actuators, and the loads were reacted at mainframe attachments located near the center of the TIBB. The loads applied to the TIBB were substantial and caused significant deformations to occur in the test fixture itself. These deformations were not measured during the test but contributed to an unsymmetric loading of the TIBB as evidenced by the experimental results (ref. 1). The deformations of the TIBB were measured with respect to the floor of the testing laboratory, and these TIBB deformations were used in the analysis to model the loading condition created by the test fixture.

A global/local approach was used to analyze the TIBB. The TIBB deformations were applied as boundary conditions to a global model of the TIBB. Deformations from the global model were used as input boundary conditions to a local model of a portion of the TIBB including the failure region. Results from the global and local analyses were compared to experimental results to validate these analytical models.

- **Test fixture response led to unquantified rigid body motions and unsymmetric loading of TIBB.**
- **Hydraulic actuator displacements and mainframe displacements at the slot and pin locations used as boundary conditions to the TIBB analysis.**
- **Experimental and analytical results used to develop the failure scenario.**
- **Global/local analysis approach was used to understand TIBB response mechanisms.**

Figure 3

Axial Surface Strain for Failure Load Case From Linear Global Analysis

Axial surface strain distributions obtained from an MSC/NASTRAN (ref. 2) global model of the TIBB are shown in figure 4. These strains correspond to the TIBB loading at failure, and this loading is referred to herein as the failure load case. The model used for the present analysis was based on a model developed by Lockheed for the TIBB and has been modified to update laminate stacking sequences and stiffener geometry. This model contains 3,885 quadrilateral, triangular, and bar elements and has 2,763 nodes. The total number of unconstrained degrees of freedom is 16,578.

The exterior surface strain distribution is shown on the TIBB global model in the upper half of the figure. These results do not indicate any unusually high exterior surface strains. A portion of the interior surface strain distribution is shown in the lower half of the figure. The interior surface strain distribution is presented for the upper cover panel region near the observed failure. These results show strains for the skin of the upper cover panel that are greater than -0.01 in./in. in the gap region. The high skin strains are caused by the flange termination and an eccentric load path that induces local bending. The observed TIBB failure extends through the gap region.

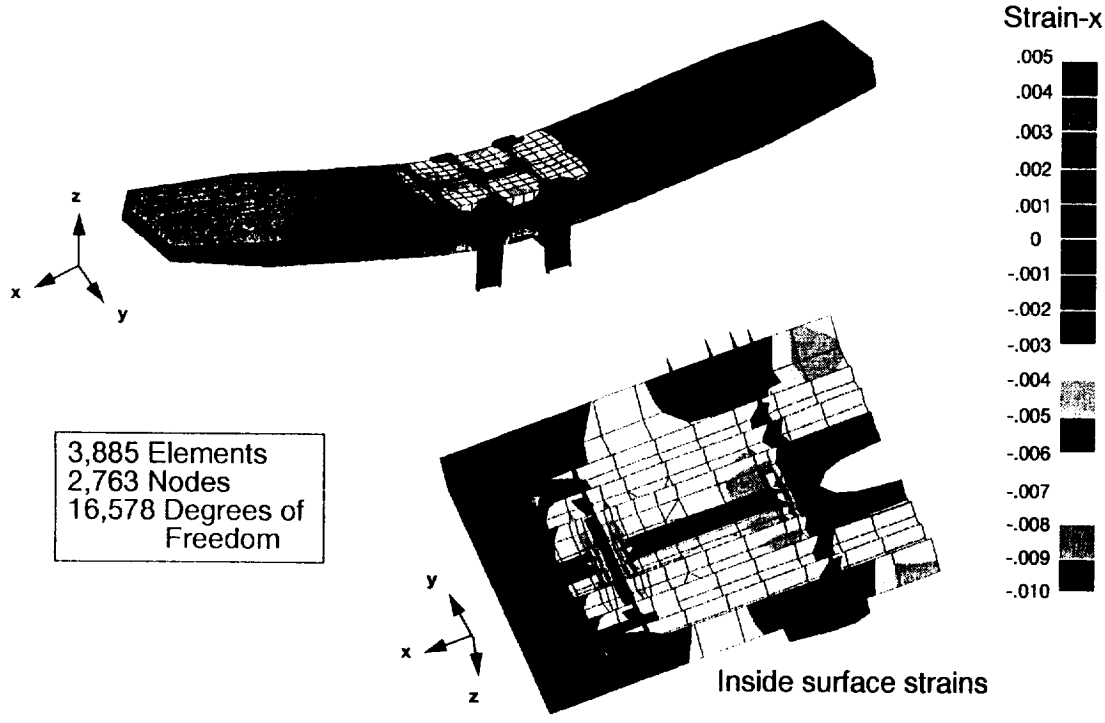

Figure 4

Finite Element Model for Local Analysis

A detailed local finite element model for half of the upper cover panel was developed to understand better the strains at the hat stiffener terminations where failure of the TIBB occurred. The local model is shown in figure 5 and consists of 4338 9-noded Assumed Natural-Coordinate Strain elements (ref. 3) resulting in approximately 88,000 degrees-of-freedom. Displacements from the global analysis were applied to all four edges of the local model as well as at the skin where the rib shear ties attached to the upper cover panel. The local analysis was performed using the COmputational MEchanics Testbed (COMET, ref. 4).

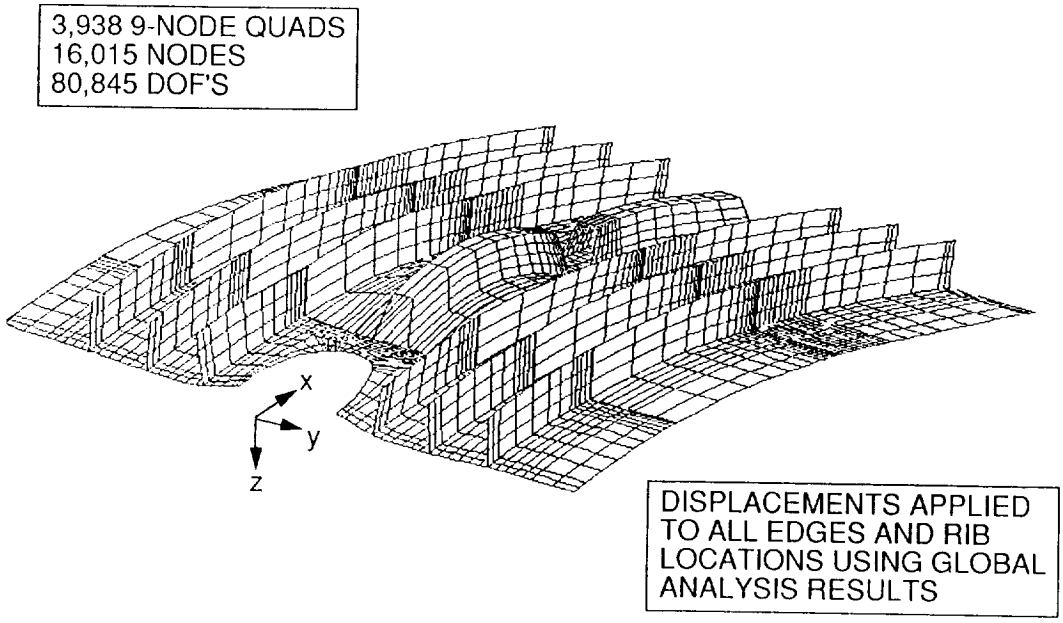

Figure 5

Axial Strains for TIBB Specimen

Axial strains for the TIBB specimen from analyses and test are presented in figure 6 for the failure load case. Three sets of analytical results are presented including local linear analysis, local nonlinear analysis, and global nonlinear analysis. The MSC/NASTRAN computer program (solution 106, V67) was used for the global nonlinear analysis. Strain results for Gages 24 and 25 are shown as open symbols on the figure. These back-to-back gages are located midway between Gap 1 and Gap 2 (see Figure 1) on the top of the hat stiffener. The strains measured by Gage 24 show that the exterior surface of the skin is in compression. The strains measured by Gage 25 show that this region of the hat stiffener is loaded in tension due to the severe bending that results when the TIBB is subjected to upbending load. As mentioned previously, the severe bending is due to the changing location of the cross-section neutral axis along the TIBB span.

The results from the local nonlinear and global nonlinear analyses agree very well with the experimental results. Nonlinear bending was predicted by both analyses. The linear analysis results underestimated the strains at Gage 25 significantly. The strain curve for Gage 25 is highly nonlinear, while the strain curve for Gage 24 is linear. This behavior is due to the fact that the neutral surface for the panel cross-section is much closer to Gage 24 than to Gage 25.

Comparisons of analytical and experimental results were made for other regions of the TIBB and for other load cases using the linear global and nonlinear local analytical models. Generally, good agreement was observed between the analytical and experimental results thereby verifying the analytical models.

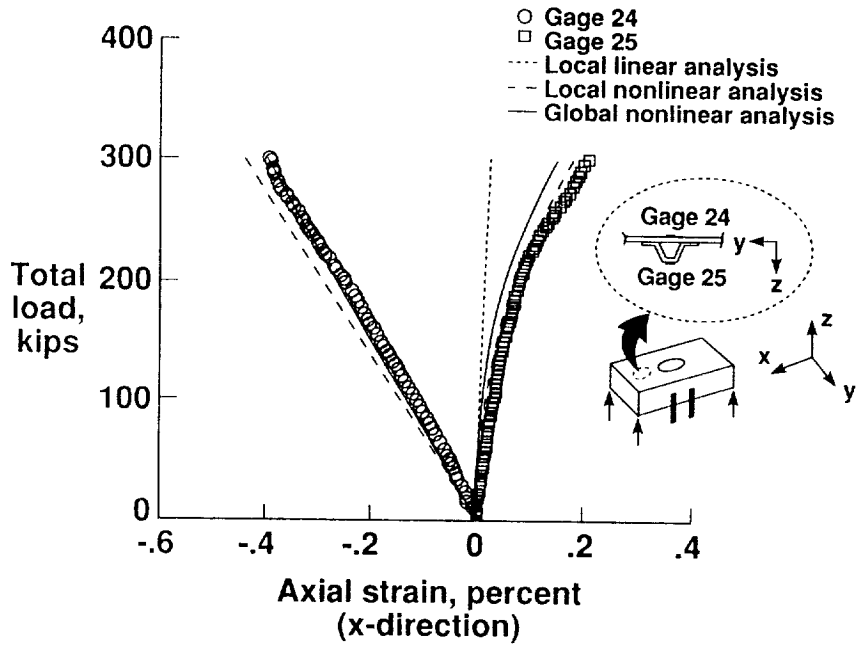

Figure 6

Failure Scenario of TIBB

The failure scenario of TIBB was developed based on the analytical results and available test results. Because the TIBB failure was catastrophic and instrumentation in the failure region was insufficient, the failure sequence could not be determined solely from the test data. The results shown on figure 7 illustrate how experimental observations were used with the verified analytical models to develop the TIBB failure scenario. Strain results along the center line of the runout hat stiffener flange from a local nonlinear analysis are plotted in the left half of the figure. This center line is shown as a dashed line on the TIBB sketch in the right half of the figure. Very high strains are found at each gap. The highest strain calculated by the analysis is found at Gap 1. The gap exterior skin surfaces are subjected to tension, and the gap interior skin surfaces are subjected to compression. These strain results indicate that the skin in the gap regions is subjected to severe bending which may cause compression or interlaminar shear failure in the laminate.

Test results for strain gages located near Gap 1 showed a significant strain change at 287 kips test load when a loud noise was heard. The TIBB was visually inspected while the load was held constant. However, no damage was observed. These observations combined with the analytical results suggest that failure initiated at Gap 1. The damage at Gap 1 may not have been detected during inspection since this gap region was not identified as a critical region for the TIBB. After inspection, the test was continued and the TIBB ultimately failed at 300 kips at Gap 2 which is also predicted to be a high stress region. Load redistibution subsequent to the failure in Gap 1 may have caused Gap 2 to become the critical stress region leading to the observed failure in Gap 2.

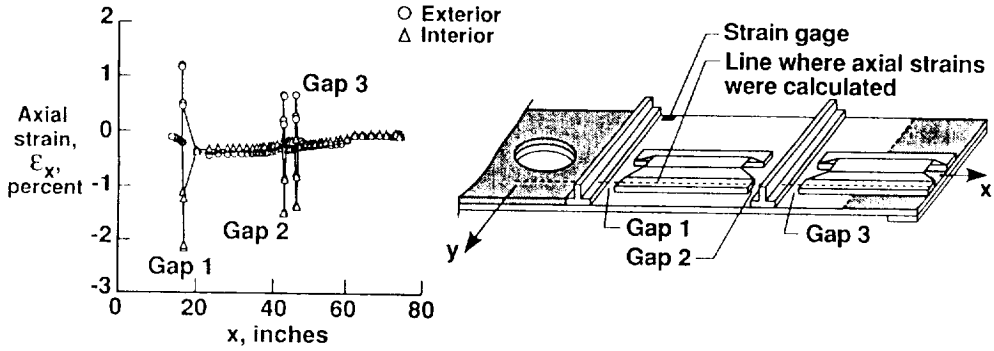

- Gap 1 is suspected to be the critical gap prior to the initial failure event
- A load noise was heard at 287 kips prior to ultimate failure. Load was held constant while the TIBB was inspected. No damage was observed.
- Based upon strain data from a gage near gap 1 the noise may have been associated with a local failure in or near gap 1. The load redistributed making gap 2 critical.
- When loading continued the TIBB ultimately failed at 300 kips in gap 2

Figure 7

Selection of Stiffener Runout Test Specimen

A Stiffener Runout Test Specimen (SRTS) was defined to simulate the response of the TIBB in the region of failure and to validate the TIBB failure scenario. The SRTS was cut from an undamaged region of the TIBB as indicated by the dashed rectangle on the illustration in figure 8. The SRTS contained gaps and similar design details as those contained in the TIBB failure region (see detail A-A). The SRTS was approximately 60 in. long and 33 in. wide and was tested in uniaxial compression.

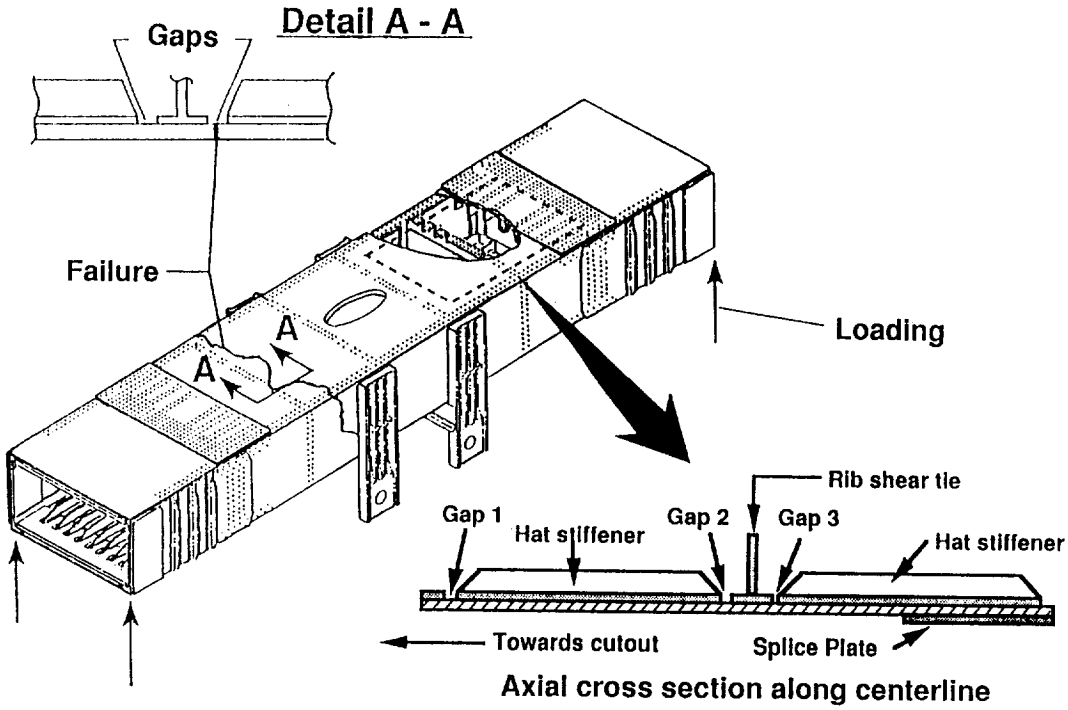

Figure 8

SRTS Specimen Deformed Geometry
Axial Compression Load = 430 kips

An extensive parametric study was performed to determine the proper test specimen geometry, loading, and boundary conditions to best simulate the response of the TIBB upper cover at failure. A half model of the SRTS was developed with approximately 32,000 degrees of freedom and is shown in figure 9. The analyses indicated that continuous knife-edge supports were required along both sides of the panel during testing and that the cap of the hat stiffener should not be loaded directly in compression. The deformed model is shown in the figure and illustrates the bending of the hat stiffener that is characteristic of the TIBB failure mode. Axial strain contours are superimposed on the deformed model, and they indicate high stresses in the gap regions.

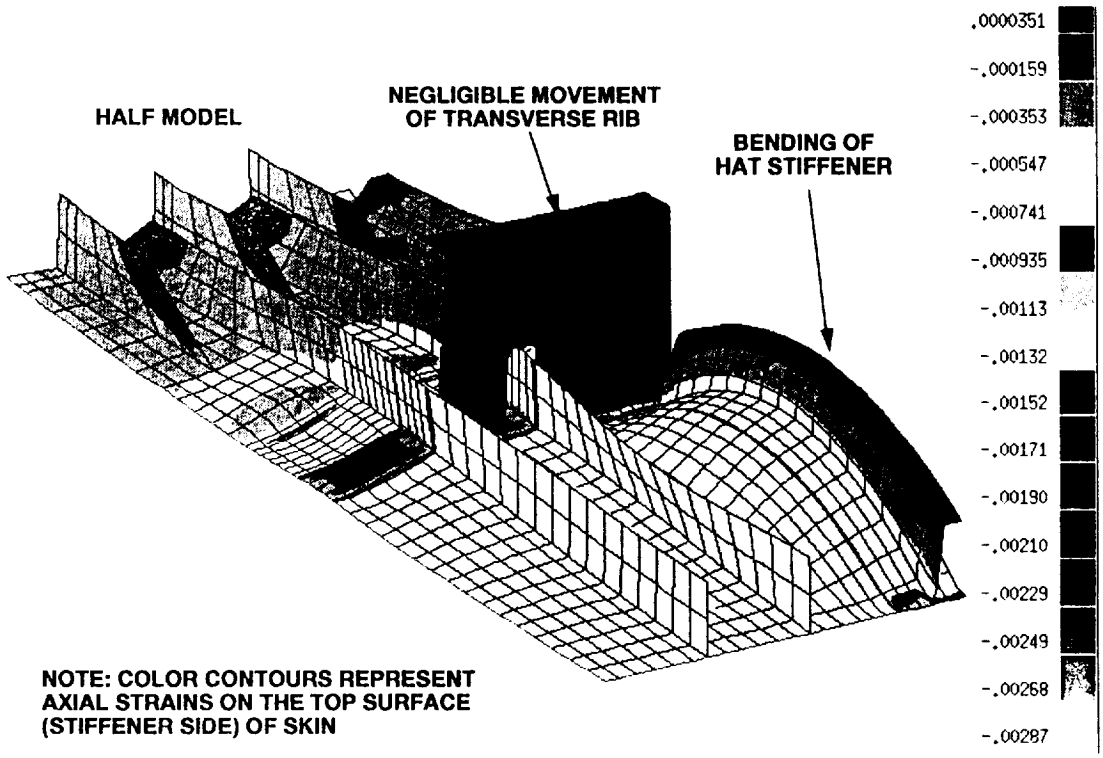

Figure 9

Test Objectives and Program for SRTS

The test objectives and program for the SRTS are outlined in figure 10. The SRTS test program was designed to correlate the response and failure mechanisms predicted by the finite element analysis with the experimental response. Preloading tests at approximately 20 to 50 percent of the predicted initial failure loads were conducted first to obtain experimental results for validating the predicted response of the SRTS and to make necessary modifications to the test setup, if needed. The specimen initial failure was predicted to occur in Gap 3 at a total load of 460 kips. After processing this information and ensuring that the response was as predicted, the SRTS was loaded to failure. Although the TIBB failed through Gap 2, the predicted SRTS failure in Gap 3 still would confirm both the severe bending failure mechanism as well as the sensitivity of stresses in a gap to the gap geometry.

- Test Objectives
  - **Simulate TIBB response and failure mechanisms**
  - **Correlate response and failure mechanisms with predictions**
- Test Program
  - **Apply 100- and 250-kip uniaxial compression load to SRTS to understand response mechanisms and validate analysis**
  - **Apply uniaxial compressive load to SRTS until failure; failure predicted at 460 kips gap 3**

Figure 10

Axial Displacement of the SRTS

Experimental results and a photograph of the SRTS are shown in figure 11. A comparison between experiment and analysis of the end shortening and axial rib displacement of the SRTS was performed. An LVDT displacement transducer was attached to the upper load platen of the test machine to measure the overall shortening of the panel as a function of applied load. Another LVDT was attached to the rib along the longitudinal centerline of the panel and at the most out-of-plane part of the rib. The measured displacement of the LVDT on the rib consists of both axial panel shortening and rib rolling.

The experimentally measured and analytically predicted end shortening of the SRTS was nearly linear to failure. The predicted end shortening was less than the measured end shortening for a given load level which implies that the predicted panel membrane stiffness was greater than the corresponding measured stiffness. The difference in panel stiffness is attributed to the coarse level of finite element discretization used in this region resulting in a stiffer structure and to the nonuniform thickness distribution along the longitudinal axis of the panel.

The experimentally measured axial rib displacement was nearly linear until approximately 500 kips of load was applied which resulted in large displacements. However, the predicted response was nearly linear to failure. The highly nonlinear response of the rib is due to the rolling of the rib. During the linear portion of the load-deflection response, the good agreement between experimental and analytical results is attributed to the high level of discretization and the uniform thickness along the length of the SRTS. However, the mechanisms that produced rib rolling were not adequately represented by the analysis.

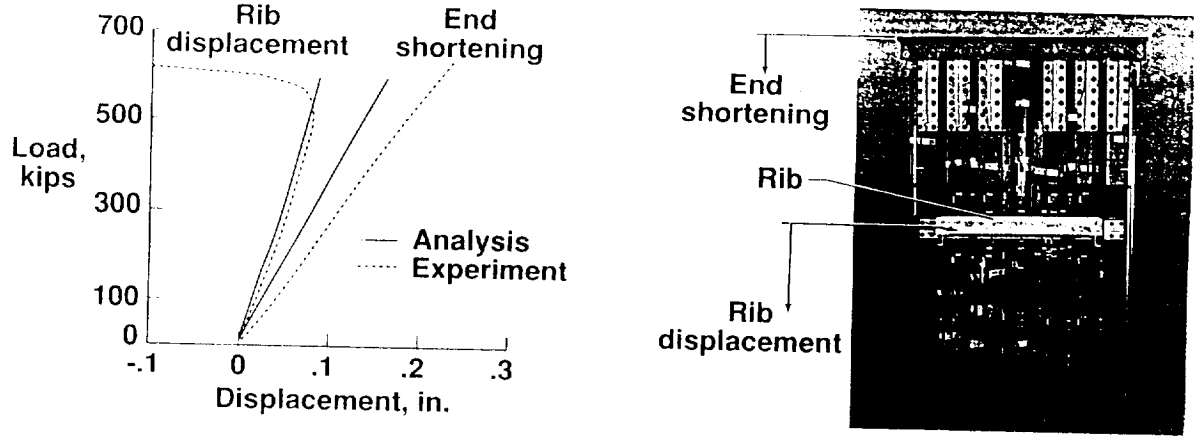

Figure 11

Global Strain Response for the SRTS

Far-field (or global) strain results are presented in figure 12. Over 190 strain gages were mounted to the SRTS to measure global strain response and the strain response in the gap and near the rib. The strain gages away from rib provide an indication of the global response of the panel and determine whether the load is evenly distributed in the panel. A comparison is made between the predicted and measured global strains. Strain gages used in this comparison were located on (A) the hat stiffener above the rib (upper hat stiffener), (B) the center of the hat stiffener below the rib (lower hat stiffener), and (C) a blade stiffener midway between the rib and the potted end. Gages were located on both the stiffener and skin sides of the SRTS to quantify any local bending.

In general, good agreement was achieved between all measured and predicted global strains. The strains below the rib (e.g., locations B and C) were more accurately predicted than strains above the rib. Considerable bending of the lower hat stiffener occurred producing a localized nonlinear response. A similar response occurred in the TIBB. The strains on the blade stiffeners were linear to failure with little or no blade stiffener bending occurring. The hat stiffener above the rib exhibited a nearly linear response to failure with little bending. The differences in response of the hat stiffeners are attributed to the local reinforcement of the skin around the upper hat stiffener.

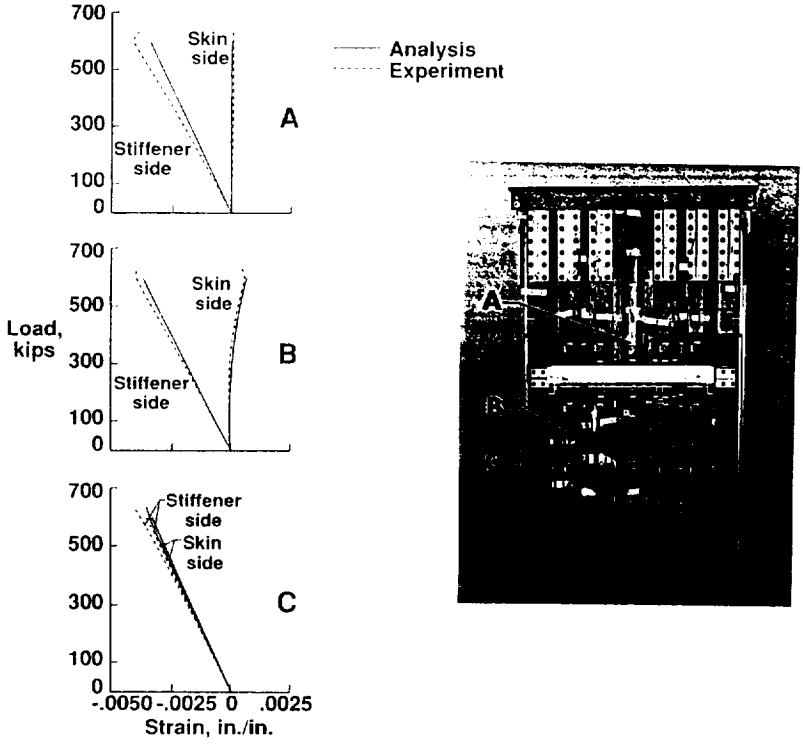

Figure 12

Strains in and Near Gaps 2 and 3

Strain results near Gaps 2 and 3 are shown in figure 13. Back-to-back strain gages were mounted on the SRTS in Gap 2, location (A), and on both sides of the rib outside of the gaps, locations (B) and (C). The purpose of these gages was to quantify the magnitude of the strains in the gap, to determine the extent of bending that occurred in the gap, and to compare these results with predictions.

Surface strains in Gap 2 did not exceed -0.8 percent. A considerable amount of bending occurred as indicated by the strain reversal occurring at approximately 500 kips. The strain outside of Gap 2, such as at locations (B) and (C), was nearly linear until the rib began to roll at approximately 500 kips. The maximum measured strain occurred at location (C) and was approximately -0.9 percent. The agreement between predicted and measured strain in the gap was poor. The poor agreement is attributed to the finite element modeling assumptions of the elements in the gap and the use of strain gages to measure strain in a region of high strain gradients. Reasonable agreement, prior to rolling of the rib, was achieved between experiment and analysis for skin side strains near the rib, however poor agreement occurred on the stiffener side.

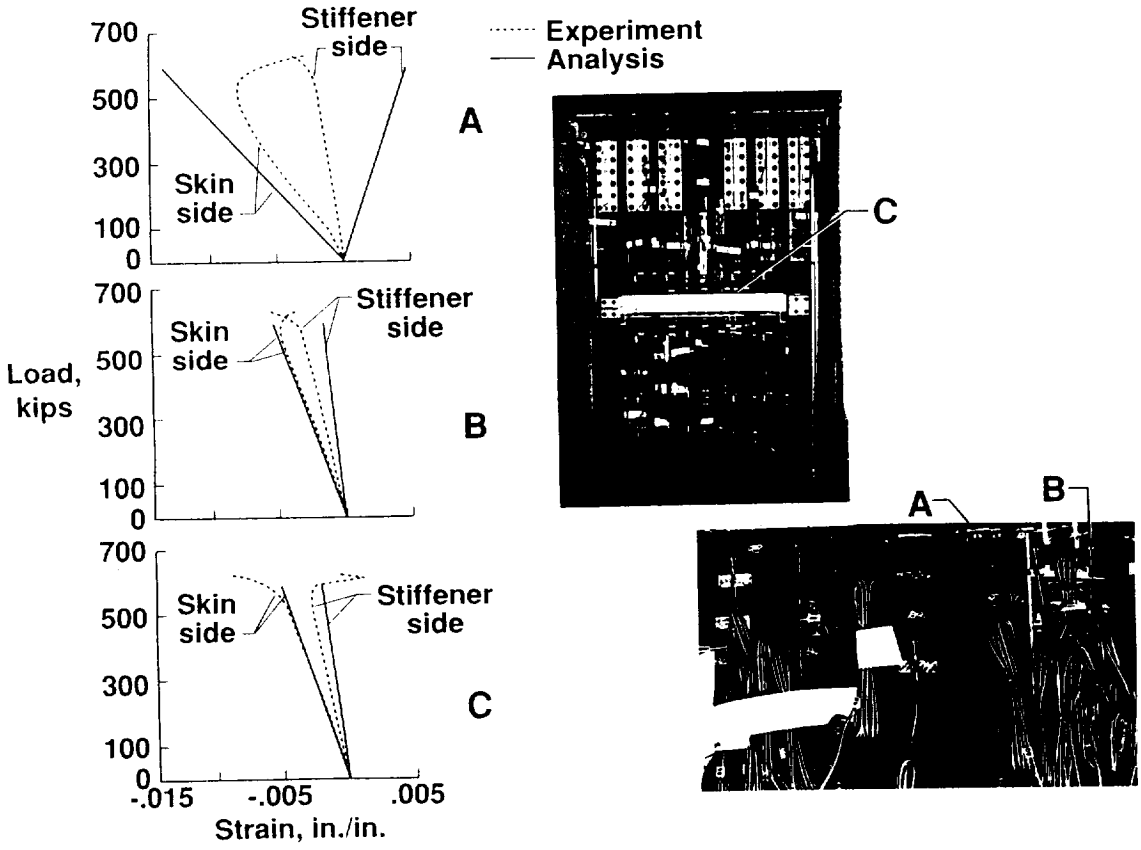

Figure 13

SRTS FAILURE SCENARIO

The SRTS failure scenario is outlined in figure 14. The response of the SRTS resembled the response of the TIBB's upper cover panel at loads below 350 kips. Due to the load path eccentricities in the SRTS, the skin in Gaps 2 and 3 formed "bucket-like" regions in Gaps 2 and 3. For loads above 350 kips the rib began to roll towards Gap 3. As the rib rolled, the "bucket" in Gap 2 began to flatten, thus relieving the stresses in Gap 2 but creating a hinge at Gap 3. Significant audible sounds were recorded at 467 and 474 kips that suggested that a local failure event had occurred. At approximately 500 kips, the rib response became nonlinear, possibly due to the local failure events and the increased bending of the hat stiffener. As loading continued, high stresses in Gap 3 precipitated final failure of SRTS at 625 kips.

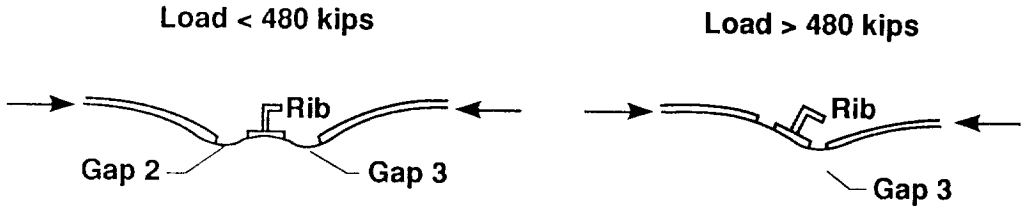

- **SRTS response resembled TIBB upper cover panel response. SRTS response beyond 350-kip load involved significant bending of the hat stiffener and rolling of the rib.**
- **SRTS response relieved stresses in gap 2 but created a hinge at gap 3.**
- **Significant audible sounds were registered at 467- and 474-kip loads that suggested local failure events.**
- **As loading continued, high stresses in gap 3 precipitated final failure of SRTS at 625 kips.**

Figure 14

Concluding Remarks

A thorough analytical and experimental study has been completed for the failure of the Technology Integration Box Beam (TIBB). Nonlinear finite element analyses were used to predict accurately the TIBB response and were verified by experimental results. Experimental and analytical results indicate that the TIBB failure initiated in Gap 1 between a rib and a terminated stiffener and that subsequent load redistribution resulted in the observed failure in Gap 2 between a rib and a terminated stiffener. A Stiffener Runout Test Specimen (SRTS) was defined to simulate the TIBB response in the failure region and to validate the TIBB failure scenario. A detailed parametric study of the SRTS was conducted prior to testing to determine the specimen geometry and boundary conditions needed to simulate the TIBB failure and to predict the SRTS response. The SRTS response and failure was observed to resemble the TIBB response and failure. The predicted SRTS response correlated reasonably well with the experimental results up to initial failure. The predicted failure mode and location for the SRTS agreed with the observations.

References

1. Shuart, M. J.; Ambur, D. R.; Davis, D. D., Jr.; Davis, R. C.; Farley, G. L.; Lotts, C. G.; and Wang, J. T.: Technology Integration Box Beam Failure Study: Status Report. Proceedings of the Second NASA Advanced Composites Technology Conference, Lake Tahoe, NV, November 4-7, 1991, NASA CP 3154, pp. 99-111.

2. Anon: MSC/NASTRAN User's Manual, Version 65, Vols. 1 and 2. MacNeal-Schwendler Corporation.

3. Park, K. C.; and Stanley, G. M.: A Curved C° Shell Element Based on Assumed Natural-Coordinate Strains. Journal of Applied Mechanics, vol. 108, 1986, pp. 278-290.

4. Knight, N. F., Jr.; and Stroud, W. J.: Computational Structural Mechanics: A New Activity at the NASA Langley Research Center. NASA TM 87612, 1985.

5. Lotts, C. G.; Greene, W. H.; McCleary, S. L.; Knight, N. F.; Paulson, S. S.; and Gillian, R. E.: Introduction to the Computational Structural Mechanics Testbed. NASA TM 89096, 1987.